Controlling chaos faster

Christian Bick,[1,2,3,a)] Christoph Kolodziejski,[1,4] and Marc Timme[1,5]
[1]*Network Dynamics, Max Planck Institute for Dynamics and Self-Organization (MPIDS), 37077 Göttingen, Germany*
[2]*Bernstein Center for Computational Neuroscience (BCCN), 37077 Göttingen, Germany*
[3]*Institute for Mathematics, Georg–August–Universität Göttingen, 37073 Göttingen, Germany*
[4]*III. Physical Institute—Biophysics, Georg–August–Universität Göttingen, 37077 Göttingen, Germany*
[5]*Institute for Nonlinear Dynamics, Georg–August–Universität Göttingen, 37077 Göttingen, Germany*

(Received 20 February 2014; accepted 5 September 2014; published online 19 September 2014)

Predictive feedback control is an easy-to-implement method to stabilize unknown unstable periodic orbits in chaotic dynamical systems. Predictive feedback control is severely limited because asymptotic convergence speed decreases with stronger instabilities which in turn are typical for larger target periods, rendering it harder to effectively stabilize periodic orbits of large period. Here, we study stalled chaos control, where the application of control is stalled to make use of the chaotic, uncontrolled dynamics, and introduce an adaptation paradigm to overcome this limitation and speed up convergence. This modified control scheme is not only capable of stabilizing more periodic orbits than the original predictive feedback control but also speeds up convergence for typical chaotic maps, as illustrated in both theory and application. The proposed adaptation scheme provides a way to tune parameters online, yielding a broadly applicable, fast chaos control that converges reliably, even for periodic orbits of large period. © *2014 AIP Publishing LLC*.
[http://dx.doi.org/10.1063/1.4895848]

Chaos control underlies a broad range of applications across physics and beyond. To successfully use chaos control schemes in applications, different robustness and convergence properties need to be considered from a practical point of view. For instance, for control to be useful in praxis, a method does not only need to guarantee convergence to the desired state, but convergence also has to be sufficiently fast. Predictive feedback control provides an easy-to-implement way to realize chaos control in discrete time dynamical systems (iterated maps). However, periodic orbits of larger periods are typically highly unstable, leading to slow convergence. Here, we systematically investigate a recently introduced extension of predictive feedback control obtained by stalling control and complement it with an adaptation mechanism. The stalling of control, i.e., repeated transient interruption of control, takes advantage of the uncontrolled chaotic dynamics, thereby speeding up convergence. Adaptation provides a way to tune the control parameters online to values which yield optimal speed. Specifically, we show how the efficiency of stalling control depends on both the local stability properties of the periodic orbits to be stabilized and the choice of control parameters. Furthermore, we derive conditions for stabilizability of periodic orbits in systems of higher dimensions. In addition to speeding up convergence, the gradient adaptation scheme presented also further increases the overall convergence reliability. Hence, adaptive stalled predictive feedback control yields an easy-to-implement, noninvasive, fast, and reliable chaos control method for a broad scope of applications.

I. INTRODUCTION

Typically, chaotic attractors contain infinitely many unstable periodic orbits.[1] The goal of chaos control is to render these orbits stable. After first being introduced in the seminal work by Ott *et al.*[2] about two decades ago, it has not only been hypothesized to be a mechanism exploited in biological neural networks[3] but it has found its way into many applications,[4,5] including chaotic lasers, stabilization of cardiac rhythms, and more recently into the control of autonomous robots.[6]

Predictive Feedback Control (PFC)[7,8] is well suited for applications: little to no prior knowledge about the system is required, it is non-invasive, i.e., control strength vanishes upon convergence, and it is very easy to implement due to the nature of the control transformation. In PFC, a prediction of the future state of the system together with the current state is fed back into the system as a control signal, similar to time-delayed feedback control.[9] In fact, it can be viewed as a special case of a recent effort to determine all unstable periodic points of a discrete time dynamical system[10,11] which has been studied and extended[12–15] for its original purpose.

In any real world application not only the existence of parameters that lead to stabilization, but also the speed of convergence is of importance. Speed is crucial, for example, if a robot is controlled by stabilizing periodic orbits in a chaotic attractor,[6] since the time it needs to react to a changing environment is bounded by the time the system needs to converge to a periodic orbit of a given period. In most of the literature, however, speed of convergence has been

a)Present address: Department of Mathematics, Rice University, MS–136, 7500 Main St., Houston, Texas 77005, USA.

overlooked. Stabilizing periodic orbits of higher periods becomes quite a challenge; due to the increasing instability of the orbits, the PFC method yields only poor performance in terms of asymptotic convergence speed even when the control parameter is chosen optimally. Any method optimizing speed within the PFC framework[16] therefore is subject to the same limitation.

In this article, we investigate Stalled Predictive Feedback Control (SPFC), a recently proposed extension of predictive feedback control that can overcome this "speed limit."[17] Here, we derive conditions for the local stability properties of periodic orbits that imply stabilizability. Furthermore, we propose an adaptation mechanism that is capable of tuning the control parameter online to reach optimal asymptotic convergence speed within the regime of convergence. The resulting adaptive SPFC method is an easy-to-implement, non-invasive, and broadly applicable chaos control method that stabilizes even periodic orbits of large periods reliably without the need to fine-tune parameter values a priori.

This article is organized as follows. In Sec. II, we formally introduce the PFC method, briefly discuss its limitations and present SPFC as an alternative. Section III is dedicated to an in-depth look at the SPFC method; we identify regimes in parameter space in which stabilization is successful. In Sec. IV, we apply our algorithm to "typical" maps with chaotic dynamics and calculate and compare convergence speeds. Adaptive methods for the control parameter are explored in Sec. V before giving some concluding remarks.

II. PRELIMINARIES

Suppose $f : \mathbb{R}^N \to \mathbb{R}^N$ is a differentiable map such that the iteration given by the evolution equation $x_{k+1} = f(x_k)$ gives rise to a chaotic attractor $A \subset \mathbb{R}^N$ with a dense set of unstable periodic orbits. We refer to such a map as a *chaotic map*. Let $\mathrm{Fix}(f) = \{x^* \in \mathbb{R}^N \,|\, f(x^*) = x^*\}$ denote the set of fixed points of f and id the identity map on $\mathbb{R}^N$. The main result of Schmelcher and Diakonos[11] reads as follows.

Proposition II.1. Suppose $\mathrm{Fix}^*(f) \subset \mathrm{Fix}(f)$ *is the set of fixed points such that both* $\mathrm{d}f|_{x^*}$ *and* $\mathrm{d}f|_{x^*} - \mathrm{id}$ *are nonsingular and diagonalizable (over* $\mathbb{C}$*). Then there exist finitely many orthogonal matrices* $M_k \in O(N)$, $k = 1, \ldots, K$, *such that we have*

$$\mathrm{Fix}^*(f) = \bigcup_{k=1}^{K} \mathcal{C}(f, M_k),$$

where the sets $\mathcal{C}(f, M_k)$ *are characterized by the property that for* $x^* \in \mathcal{C}(f, M_k)$ *there exists* $\mu \in (0, 1)$ *such that* x^* *is a stable fixed point of the map* $g_{\mu,1}$ *obtained by the transformation* $S(\mu, M_k) : f \mapsto \mathrm{id} + \mu M_k (f - \mathrm{id}) = g_{\mu,1}$.

A. Predictive feedback control

This result may be cast into a control method. Let $\mathbb{N}$ denote the set of natural numbers. A periodic orbit of period $p \in \mathbb{N}$ is a fixed point of the pth iterate of f denoted by

$$f_p := f^{\circ p} = \underbrace{f \circ \cdots \circ f}_{p \text{ times}},$$

and therefore we use the terms fixed point and periodic orbit interchangeably depending on what is convenient in the context. Let $\mathrm{Per}(f) = \cup_{p \in \mathbb{N}} \mathrm{Fix}(f_p)$ denote the set of all periodic points of f. Define the set of periodic orbits of minimal period p as $\mathrm{Fix}(f, p) = \{x^* \in \mathrm{Fix}(f_p) \,|\, f^{\circ q}(x^*) \neq x^* \text{ for } q < p\}$. Furthermore, we define $\mathrm{Fix}^*(f, p) = \mathrm{Fix}(f, p) \cap \mathrm{Fix}^*(f_p)$. Predictive feedback control is now a consequence of Proposition II.1 by replacing f with f_p.

Corollary II.2. Let $p \in \mathbb{N}$. *For every* $x^* \in \mathrm{Fix}_g^*(f, p) := \mathrm{Fix}^*(f, p) \cap (\mathcal{C}(f_p, \mathrm{id}) \cup \mathcal{C}(f_p, -\mathrm{id}))$ *there exists a* $\mu \in (-1, 1)$ *such that* x^* *is a stable fixed point of the* predictive feedback control *method given by the iteration*

$$x_{k+1} = g_{\mu,p}(x_k) := f_p(x_k) + \eta(x_k - f_p(x_k))$$

with $\eta = 1 - \mu$ *and control perturbation* $c_{\mu,p}(x) = \eta(x_k - f_p(x_k))$.

The elements of $\mathrm{Fix}_g^*(f, p)$ are referred to as *PFC-stabilizable* periodic orbits of period p. The cardinality of the set $\mathrm{Fix}_g^*(f, p)$ depends on the chaotic map f and contains roughly half of the periodic orbits of a given period in two-dimensional systems.[11,12]

Fix $x^* \in \mathrm{Fix}^*(f, p)$. Local stability of $g_{\mu,p}$ at x^* is readily computed. Let $\mathrm{d}f|_x$ denote the total derivative of f at x and suppose that $\lambda_j, j = 1, \ldots, N$ are the eigenvalues of the linearization. The derivative of $g_{\mu,p}$ at x^* evaluates to $\mathrm{d}g_{\mu,p}|_x = \mathrm{id} + \mu(\mathrm{d}f_p|_x - \mathrm{id})$. Hence, stability is determined by the eigenvalues of $\mathrm{d}g_{\mu,p}|_{x^*}$ given by

$$\kappa_j(\mu) = 1 + \mu(\lambda_j - 1) \tag{1}$$

for $j = 1, \ldots, N$. Hence, $x^* \in \mathrm{Fix}_g^*(f, p)$ iff there exists a $\mu_0 \in (-1, 1)$ such that the spectral radius $\varrho(\mathrm{d}g_{\mu_0,p}|_{x^*}) = \max_{j=1,\ldots,N} |\kappa_j(\mu_0)|$ is smaller than one. In particular, for a two-dimensional system, these are the periodic orbits of saddle type[12] with stable direction $\lambda_1 \in (-1, 1)$ and $\lambda_2 < -1$. Note that optimal convergence speed is achieved for the value of μ which corresponds to the minimal spectral radius.

B. Speed limit of predictive feedback control

For increasing instability, however, the optimal convergence speed becomes increasingly slow.[17] This applies, in particular, to periodic orbits of larger periods as the periodic orbits become increasingly unstable on average[18] and asymptotic convergence speed decreases. Let $\varrho_{\min}^g(x^*) = \inf_\mu \varrho(\mathrm{d}g_{\mu,p}|_{x^*})$ denote the spectral radius of the linearization at a periodic orbit x^* for the optimal parameter value and # the cardinality of a set. The slowdown of PFC can be explicitly calculated by evaluating the functions

$$\underline{\rho}_g(p) = 1 - \min_{x^* \in \mathrm{Fix}_g^*(f,p)} \varrho_{\min}^g(x^*), \tag{2a}$$

$$\rho_g(p) = 1 - \frac{1}{\#\left(\mathrm{Fix}_g^*(f,p)\right)} \sum_{x^* \in \mathrm{Fix}_g^*(f,p)} \varrho_{\min}^g(x^*), \tag{2b}$$

$$\bar{\rho}_g(p) = 1 - \max_{x^* \in \mathrm{Fix}_g^*(f,p)} \varrho_{\min}^g(x^*), \tag{2c}$$

that quantify to the best, average, and worst asymptotic convergence speed for all periodic orbits of a given period, respectively.

The slowdown becomes explicit in specific examples. We evaluated these functions for a map which describes the evolution of an artificial neural network referred to as a neuromodule.[19] For a two dimensional neuromodule, let $l_{11}=-22$, $l_{12}=5.9$, $l_{21}=-6.6$, and $l_{22}=0$ and define the sigmoidal function $\sigma(x)=(1+\exp(-x))^{-1}$. The dynamics are given by the map $f:\mathbb{R}^2\to\mathbb{R}^2$ where

$$f(x_1,x_2)=(l_{11}\sigma(x_1)+l_{12}\sigma(x_2)-3.4,\\ l_{21}\sigma(x_1)+l_{22}\sigma(x_2)+3.8). \tag{3}$$

The values of the functions (2) are depicted in Figure 1. One can clearly see that even the lower bound on asymptotic convergence speed for the PFC method, corresponding to the smallest spectral radius as determined by $1-\underline{\rho}_g$, approaches one exponentially on average for increasing periods. This scaling of convergence speed of PFC is quite typical; other maps with chaotic attractors, such as the Hénon map, exhibit a similar behavior when subject to PFC.[17]

C. Stalled predictive feedback chaos control

By making use of the uncontrolled dynamics, i.e., "stalling control," it was recently shown that this speed limit may be overcome.[17] Stalled predictive feedback control scheme is an extension of standard predictive feedback control. For a map $\psi:\mathbb{R}^N\to\mathbb{R}^N$, define the "zeroth iterate" by $\psi^{\circ 0}:=\mathrm{id}$.

Definition II.3. Suppose that the iteration of $F:\mathbb{R}^N\to\mathbb{R}^N$ *defines a dynamical system. For* $M_k\in\{\pm\mathrm{id}\}$ *and* $\mu\in\mathbb{R}$ *let* $S(\mu,M_k)(F)=\mathrm{id}+\mu M_k(F-\mathrm{id})=:G_\mu$ *denote the map obtained by applying the predictive feedback control transformation; cf. Proposition II.1. For parameters* $m,n\in\mathbb{N}_0=\mathbb{N}\cup\{0\}$ *and* $\mu\in\mathbb{R}$*, the iteration of*

$$H_\mu^{(m,n)}=(F)^{\circ n}\circ(G_\mu)^{\circ m} \tag{4}$$

is referred to as stalled predictive feedback control.

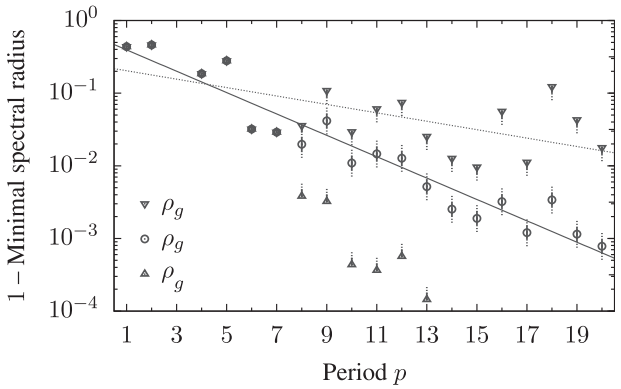

FIG. 1. Since the minimal spectral radius converges to 1, the best, average, and worst asymptotic convergence speeds over all periodic points of a given period decrease with increasing period. Here, the values of $\underline{\rho}_g(p),\rho_g(p),\bar{\rho}_g(p)$ are plotted for the two-dimensional map (3). To visualize the decrease, we fit $\rho_g(p)$ (average minimal spectral radius; solid line) and best $\bar{\rho}_g(p)$ (best minimal spectral radius; dotted line) spectral radius with an exponential function; cf. Sec. IV A.

The function $H_\mu^{(m,n)}$ defined above stalls predictive feedback control in the following sense. In the PFC method, the control signal is applied at every point in time. By iterating $H_\mu^{(m,n)}$ we "stall" the application of the control perturbation by adding extra evaluations of the original, uncontrolled map F.

Henceforth, we adopt the period-dependent notation introduced above: the uncontrolled dynamics were given by iterating $f:\mathbb{R}^N\to\mathbb{R}^N$ and the PFC transformed map is denoted by $g_{\mu,p}$. Stalled predictive feedback control is given by the iteration of

$$h_{\mu,p}=h_{\mu,p}^{(m,n)}:=(f_p)^{\circ n}\circ(g_{\mu,p})^{\circ m}, \tag{5}$$

where $m,n\in\mathbb{N}_0$ are parameters. By definition, we have $h_{\mu,p}^{(0,1)}=f_p$ and we recover the original PFC method for $h_{\mu,p}^{(1,0)}=g_{\mu,p}$. In general, we will omit the superscript (m,n) unless the choice is important.

III. STABILITY OF STALLED PREDICTIVE FEEDBACK CHAOS CONTROL

The stability of a periodic orbit in the controlled system depends on its stability properties for the uncontrolled dynamics. In this section, we derive criteria for a periodic orbit to be stabilizable for stalled predictive feedback control.

A. Local stability of periodic orbits for $h_{\mu,p}$

The local stability properties of $h_{\mu,p}$ can be calculated from f_p and $g_{\mu,p}$. By definition, we have $\mathrm{Fix}(f_p)\subset\mathrm{Fix}(h_{\mu,p})$. Suppose that $x^*\in\mathrm{Fix}^*(f,p)$ and the eigenvalues of $\mathrm{d}f_p|_{x^*}$ are given by λ_j where $j=1,\ldots,N$. Note that the eigenvectors of $\mathrm{d}g_{\mu,p}|_{x^*}$ and $\mathrm{d}f_p|_{x^*}$ are the same. Hence, the local stability properties of $h_{\mu,p}$ are readily computed from the λ_j and the local stability properties of the PFC transformed map $g_{\mu,p}$ as given by (1). The eigenvalues of the Jacobian of $h_{\mu,p}$ at x^* evaluate to

$$\Lambda_j=\lambda_j^n\kappa_j(\mu)^m=\lambda_j^n(1+\mu(\lambda_j-1))^m$$

for $j=1,\ldots,N$. Hence, local stability at x^* is given by the spectral radius

$$\varrho(\mathrm{d}h_{\mu,p}|_{x^*})=\max_{j=1,\ldots,N}|\Lambda_j|.$$

If all eigenvalues are of modulus smaller than one, the fixed point x^* is stable for $h_{\mu,p}$. In other words, a periodic orbit $x^*\in\mathrm{Fix}^*(f,p)$ is called *SPFC-stabilizable* if there are parameters $m,n\in\mathbb{N}_0$ and $\mu\in(-1,1)$ such that

$$\varrho(\mathrm{d}h_{\mu,p}^{(m,n)}|_{x^*})<1.$$

Let $\mathrm{Fix}_h^*(f,p)$ denote the set of SPFC-stabilizable periodic orbits and, clearly, $\mathrm{Fix}_g^*(f,p)\subset\mathrm{Fix}_h^*(f,p)$, that is, every PFC-stabilizable periodic orbit is also SPFC-stabilizable.

To compare the "performance" of stalled predictive feedback control with that of original predictive feedback control, we have to rescale the stability properties. Since $h_{\mu,p}^{(m,n)}$ contains $n+m$ evaluations of f_p, we take the $(m+n)$th root to obtain functions

$$\hat{l}_j(m,n,\mu) = |\lambda_j^n\big(1+\mu\big(\lambda_j-1\big)\big)^m|^{\frac{1}{m+n}},$$

where $j=1, \ldots, N$. With the parameter $\alpha = \frac{n}{m+n}$, we thus obtain an equivalent set of functions

$$l_j(\alpha,\mu) = |\lambda_j|^{\alpha}|(1+\mu(\lambda_j-1))|^{1-\alpha} \tag{6}$$

for $j=1, \ldots, N$ which determine the local stability properties of $h_{\mu,p}$ rescaled to a single evaluation of f_p. Conversely, for any rational $\alpha \in [0,1] \cap \mathbb{Q}$, we obtain a pair (m, n). In the following, we refer to both α and the pair m, n as *stalling parameters*, depending what is convenient in the context. When using the stalling parameter α, we may also write $h^{\alpha}_{\mu,p}$.

Rescaled local stability of stalled predictive feedback control for a given periodic orbit $x^* \in \mathrm{Fix}^*(f,p)$ of period p is hence determined by the *stability function*

$$\varrho_{x^*}(\alpha,\mu) = \max_{j=1,\ldots,N} l_j(\alpha,\mu). \tag{7}$$

In comparison with the original predictive feedback control, stalled predictive feedback control depends on two parameters: the control parameter μ and the stalling parameter α.

B. Conditions for stabilizability

To derive conditions for SPFC-stabilizability, consider some general properties of functions of type (6). Fix $w \in \mathbb{C}^{\times} := \mathbb{C}\backslash\{0\}$. Let $\mathbf{S}^1 := \{z \in \mathbb{C} \,|\, |z|=1\} \cong \mathbb{R}/2\pi\mathbb{Z}$ denote the unit circle. We will choose a realization to describe elements of $\mathbf{S}^1$ depending on what is convenient in the context. Consider the function $L_w : \mathbb{R}^2 \to \mathbb{R}$ given by

$$L_w(\alpha,\mu) := |w|^{\alpha}|1+\mu(w-1)|^{1-\alpha}.$$

By definition, we have $L_w(0,\,0)=1$ and in a sufficiently small open ball V around $(0,\,0)$, the function L_w is differentiable and the derivative is bounded away from zero. Hence, in this ball the curve defined by

$$V_0 := \{(\alpha,\mu) \in V \,|\, L_w(\alpha,\mu) = 1\}$$

is a one-dimensional submanifold of $\mathbb{R}^2$. If V is chosen small enough, it may be written as a disjoint union

$$V = V_0 \cup V_+ \cup V_-,$$

where $V_+ = \{(\alpha,\mu) \in V \,|\, L_w(\alpha,\mu) > 1\}$ and $V_- = \{(\alpha,\mu) \in V \,|\, L_w(\alpha,\mu) < 1\}$.

The goal is to get a linearized description close to the origin. Let grad denote the gradient and $\langle \cdot, \cdot \rangle$ the usual Euclidean scalar product. Define the line

$$\gamma(w) = \{x \in \mathbb{R}^2 \,|\, \langle \mathrm{grad}(L_w)|_{(0,0)}, x\rangle = 0\}, \tag{8}$$

which is tangent to V_0 at the origin. Let

$$\mathcal{H} := \{x \in \mathbb{R}^2 | \langle \mathrm{grad}(L_w)|_{(0,0)}, x\rangle < 0\}$$

denote one of the half planes defined by the line $\gamma(w)$. Moreover, the sets $Q_j := \left(\frac{(j-1)\pi}{2}, \frac{j\pi}{2}\right)$ for $j \in \{1,\,2,\,3,\,4\}$ denote the open segments of $\mathbf{S}^1$ that lie in one of the four quadrants of $\mathbb{R}^2$.

Definition III.1. Suppose that $w \in \mathbb{C}^{\times}$. The connected subset $C_w := \mathcal{H} \cap \mathbf{S}^1$ is called the domain of stability of w. For a tuple $\tilde{w} = (w_1, \ldots, w_N) \in (\mathbb{C}^{\times})^N$ define the domain of stability to be

$$C_{\tilde{w}} := \bigcap_{k=1}^{N} C_{w_k}. \tag{9}$$

If $C_{\tilde{w}} \cap \overline{(Q_1 \cup Q_4)} \neq \varnothing$ then the tuple $\tilde{w}$ is called stabilizable.

In a sufficiently small neighborhood $U \subset V$ of the origin, the "linearized" version of V_- is given by the set $\mathcal{H} \cap U$.

Lemma III.2. If the domain of stability C_w of a tuple $w = (w_1, \ldots, w_N) \in (\mathbb{C}^{\times})^N$ is nonempty then there exist $(\mu_0,\, \alpha_0)$ such that $L_{w_j}(\mu_0, \alpha_0) < 1$ for all $j=1, \ldots, N$. If the tuple w is stabilizable then α_0 may be chosen such that $\alpha_0 \geq 0$.

Proof. Suppose that V_- and $\mathcal{H}$ are defined as above. Because of continuity, for every $w \in \mathbb{C}^{\times}$ there exists an open ball $B_w \subset V_- \cap \mathcal{H}$ that is tangent to the origin. If a tuple $\tilde{w} = (w_1, \ldots, w_N)$ has nonempty domain of stability $C_{\tilde{w}}$ then

$$B := \bigcap_{j=1}^{N} B_{w_j} \neq \varnothing.$$

By construction, any $(\mu_0,\, \alpha_0) \in B$ has the desired property.

If in addition, w is stabilizable then the intersection $B \cap \{(x,y) \in \mathbb{R}^2 \,|\, x \geq 0\}$ is not empty. This proves the second assertion. □

The domain of stability is determined by the gradient of L_w at the origin. Let ln denote the (real) natural logarithm. We have $\mathrm{grad}(L_w)|_{(0,0)} = (\ln|w|, \mathrm{Re}(w)-1)$. Define

$$\begin{aligned} R_1 &:= \{z \in \mathbb{C} \,|\, \mathrm{Re}(z) > 1\},\\ R_2 &:= \{z \in \mathbb{C} \,|\, |z| < 1\},\\ R_3 &:= \{z \in \mathbb{C} \,|\, |z| > 1,\, \mathrm{Re}(z) < 1\}. \end{aligned}$$

These regions are sketched in Figure 2(a). If $w \in R_1$ then $\|\mathrm{grad}(L_w)|_{(0,0)}\|^{-1} \cdot \mathrm{grad}(L_w)|_{(0,0)} \in Q_1$ and therefore $Q_3 \subset C_w$. Similarly, if $w \in R_2$ then $Q_1 \subset C_w$ and if $w \in R_3$ then $Q_2 \subset C_w$ (Figures 2(b)–2(d)). For w on the boundary of the R_k, the gradient lies on one of the coordinate axes and we obtain similar conditions.

These observations have implications for stabilizability for a tuple $(w_1,\ldots, w_N)$: if for any fixed $k \in \{1,\,2,\,3\}$ all $w_j \in R_k$ for $j=1,\ldots,N$ then the tuple is stabilizable. Furthermore, if either $w_j \in R_1 \cup R_3$ or $w_j \in R_2 \cup R_3$ for all $j=1, \ldots, N$ then the tuple is stabilizable. For any other combination, the condition of stabilizability is more difficult; in two dimensions linear dependence of the gradients tells us for $(w_1,\, w_2)$ with $w_1 \in R_1$ and $w_2 \in R_2$ the tuple is stabilizable iff

$$\ln(|w_2|)\mathrm{Re}(w_1) \neq \ln(|w_1|)\mathrm{Re}(w_2). \tag{10}$$

Note that this condition is satisfied for a set of full Lebesgue measure.

Remark III.3. Note that stabilizability is not affected by taking the complex conjugate. Hence, stabilizability of a

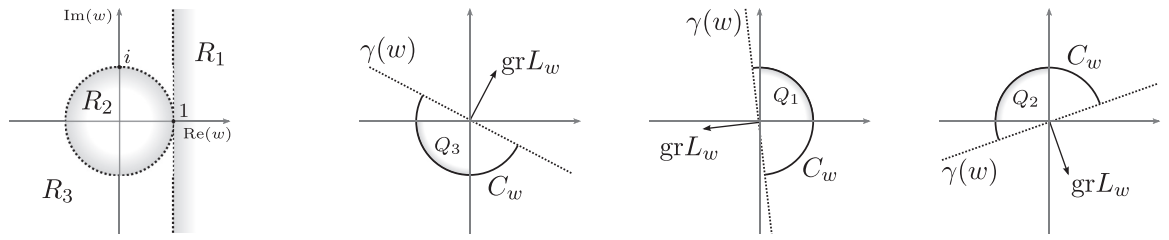

(a) Complex plane (b) $w \in R_1$ (c) $w \in R_2$ (d) $w \in R_3$

FIG. 2. Stabilizability regions for $w \in \mathbb{C}$ are shown in panel (a) and the corresponding domains of stability C_w, as given by (9), for the three cases in panels (b)–(d). Here, $\mathrm{gr}L_w = \mathrm{grad}(L_w)|_{(0,0)}$.

tuple of nonzero complex numbers as defined in Definition III.1 does not change when an entry of the tuple is replaced by its complex conjugate.

For $w=0$, the function L_0 has a discontinuity at $\alpha=0$. In case $\alpha>0$, we have $L_0(\alpha, \mu)=0$ and for $\alpha=0$ and $\mu \in (-1, 1)$, we have $L_0(0, \mu)=1-\mu$. Therefore, define the domain of stabilizability of zero to be $C_0 = \left\{0, \frac{\pi}{2}\right\} \cup Q_1 \cup Q_4$. For $\alpha>0$, stabilizability of a tuple with one component equal to zero may be reduced to stabilizability of the "reduced" tuple where the zero entry is omitted.

With the notation as above, we are now able to relate these general results to the local stability properties of a given periodic orbit.

Definition III.4. Suppose that $x^* \in \mathrm{Fix}^*(f,p)$ is a periodic orbit of f and suppose that the eigenvalues of $\mathrm{d}f_p|_{x^*}$ are given by λ_j with $j=1, \ldots, N$. The periodic orbit is called locally stabilizable if the tuple $\lambda=(\lambda_1, \ldots, \lambda_N)$ is stabilizable as a tuple, as defined in Definition III.1.

This definition links the notion of stabilizability of a tuple defined above and the local dynamics close to a periodic orbit. Recall the notion of uniform hyperbolicity.[1] Suppose that a differentiable function f defines a discrete time dynamical system on $\mathbb{R}^N$. We call an f-invariant set $A \subset \mathbb{R}^N$ hyperbolic if for every $x \in A$ no eigenvalue of $\mathrm{d}f|_x$ is of absolute value one.

Proposition III.5. Suppose that the chaotic map $f: \mathbb{R}^N \to \mathbb{R}^N$ gives rise to a hyperbolic attractor and for $x^* \in \mathrm{Fix}^*(f, p)$ let $\lambda=(\lambda_1,\ldots,\lambda_N)$ denote the eigenvalues of $\mathrm{d}f_p|_{x^*}$. If x^* is locally stabilizable then x^* is SPFC-stabilizable. Moreover, if the domain of stability C_λ satisfies

$$\left\{\frac{\pi}{2}, \frac{3\pi}{2}\right\} \cap C_\lambda \neq \varnothing,$$

then x^* is PFC-stabilizable.

Proof. If a periodic orbit x^* is locally stabilizable, then tuple λ is stabilizable. Thus, according to Lemma III.2, there are parameters (α_0, μ_0) such that $L_{\lambda_j}(\alpha_0, \mu_0)<1$ for all $j=1, \ldots, N$ simultaneously. Recall that local stability of $h^{\alpha_0}_{\mu_0,p}$ at x^* is given by $l_j(\alpha,\mu)=L_{\lambda_j}(\alpha,\mu)$ according to Eq. (6). Therefore, local stability of a periodic orbit is equivalent to the existence of parameters (α_0, μ_0) with $\alpha_0 \geq 0$ and

$$\varrho(\mathrm{d}h^{\alpha_0}_{\mu_0,p}|_{x^*}) < 1,$$

which proves the first statement.

If $\left\{\frac{\pi}{2}, \frac{3\pi}{2}\right\} \cap C_\lambda \neq \varnothing$ then there exists a parameter μ_0 such that $\varrho(\mathrm{d}h^0_{\mu_0,p}|_{x^*}) < 1$. Since stalled predictive feedback control reduces to classical predictive feedback control for a stalling parameter of $\alpha=0$, the claim follows. □

The conditions derived for stabilizability of tuples translate directly into conditions on the local stability properties of a periodic orbit. For dynamics in two dimensions, we obtain the following immediate consequence.

Corollary III.6. Suppose that $f: \mathbb{R}^2 \to \mathbb{R}^2$ is a chaotic map where all periodic orbits $x^* \in \mathrm{Per}(f)$ are of saddle type with eigenvalues λ_1, λ_2 that satisfy condition (10), i.e., we have

$$\ln(|\lambda_2|)\mathrm{Re}(\lambda_1) \neq \ln(|\lambda_1|)\mathrm{Re}(\lambda_2).$$

Then all periodic orbits $x^* \in Per(f)$ are SPFC-stabilizable.

Note that the number of constraints for stabilizability grows with increasing dimension of the dynamical system. In order to determine the absolute number of periodic orbits which are stabilizable for higher dimensional systems, a more detailed knowledge about the "average" local stability properties of periodic orbits is needed.

Since the system is real, complex eigenvalues of the derivative will always come in complex conjugate pairs. According to Remark III.3 above, this actually results in an effective decrease in the number of constraints.

C. A geometric interpretation

The local stability considerations also explain why stalled predictive feedback control increases asymptotic convergence speed.[17] Consider a periodic orbit x^* of saddle type in a two-dimensional system where contraction along the stable direction is given by $\lambda_1 \in (-1, 1)$ and expansion along the unstable manifold by $\lambda_2 < -1$. As discussed above, these are the PFC-stabilizable periodic orbits. Suppose that $\mu_{\mathrm{opt}} > 0$ is the value of the control parameter for which the spectral radius of the linearization of the PFC-transformed map $g_{\mu,p}$ takes its minimum. For $\lambda_2 \ll -1$, we have $\mu_{\mathrm{opt}} \approx 0$ and therefore $\kappa_1(\mu_{\mathrm{opt}}) \approx 1$ determines the asymptotic convergence speed of the dominating direction if the periodic orbit is stabilized. Therefore, the trajectory will approach the periodic orbit along the direction corresponding to λ_1; cf. Figure 3. The slowdown of predictive feedback control is caused by the fact that for highly unstable periodic orbits, the trajectories converge to the originally stable manifold along which convergence is slow in the transformed system.

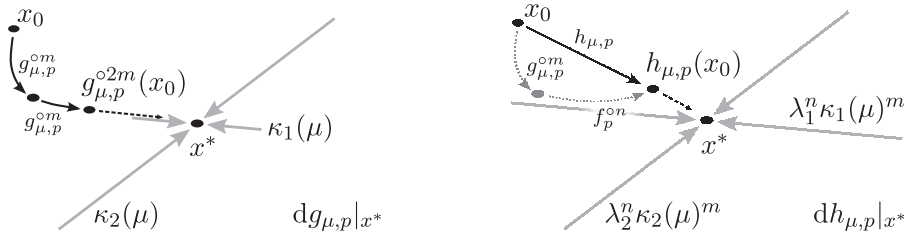

FIG. 3. Why stalling chaos control speed up convergence. Iteration of $g_{\mu,p}$ takes a trajectory to the periodic orbit x^* slowly along the direction of the originally stable manifold (panel (a)). Stalling control accelerates convergence by taking advantage of the fast convergence speed along the stable manifold (panel (b)) leading to fast overall convergence speed. The length of the gray arrows illustrates convergence speed as they scale inversely with the corresponding value of the eigenvalue.

Stalling PFC exploits exactly this property. First, iteration of $g_{\mu,p}$ takes the trajectory closer to the stable manifold. Second, iteration of f_p leads to fast convergence along the stable manifold while diverging from the stable manifold; cf. Figure 3. Thus, asymptotic convergence speed of $h_{\mu,p}$ is increased by making use of the (increasing) stability of the stable direction. For given stalling parameters m, n, the optimal value of the control parameter μ is close to the zero of $\kappa_2(\mu)$. For this value, convergence to the stable direction is strongest, taking full advantage of the fast convergence given by λ_1 along the stable manifold of the chaotic map f. The question of how to choose the stalling parameters m, n will be addressed in Sec. IV.

IV. CONVERGENCE SPEED FOR CHAOTIC MAPS

In Sec. III, we analyzed the stability properties of the SPFC method for periodic orbits in dependence of their stability properties. The improvements due to stalling can be calculated explicitly for some "typical" two and three-dimensional chaotic maps.

With $\varrho_{\min}^h(x^*) = \inf_{\mu,\alpha} \varrho_{x^*}(\alpha,\mu)$ denoting the rescaled stability of the linearization for the optimal parameter values, we calculated the functions

$$\bar{\rho}_h(p) = 1 - \min_{x^* \in \mathrm{Fix}_h^*(f,p)} \varrho_{\min}^h(x^*), \tag{11a}$$

$$\rho_h(p) = 1 - \frac{1}{\#\left(\mathrm{Fix}_h^*(f,p)\right)} \sum_{x^* \in \mathrm{Fix}_h^*(f,p)} \varrho_{\min}^h(x^*), \tag{11b}$$

$$\underline{\rho}_h(p) = 1 - \max_{x^* \in \mathrm{Fix}_h^*(f,p)} \varrho_{\min}^h(x^*) \tag{11c}$$

numerically in the same fashion as (2) to assess the scaling of optimal asymptotic convergence speed of stalled predictive feedback control for a given chaotic map across different periods. That is, for every periodic orbit of f of minimal period p, we calculated the spectral radius at the optimal parameter values and then took the minimum, maximum, and mean of these values. In particular, $1 - \underline{\rho}_h$ is the upper limit and $1 - \bar{\rho}_h$ is the lower limit for the best asymptotic convergence speed of all SPFC-stabilizable periodic orbits of a given period p rescaled to one evaluation of f_p.

The increase in the number of stabilizable orbits for PFC and SPFC can be quantified by looking at the fractions of stabilizable periodic orbits that are given by

$$\nu_h(p) = \frac{\#\left(\mathrm{Fix}_h^*(f,p)\right)}{\#(\mathrm{Fix}(f,p))} \quad \text{and} \quad \nu_g(p) = \frac{\#\left(\mathrm{Fix}_g^*(f,p)\right)}{\#(\mathrm{Fix}(f,p))}, \tag{12}$$

respectively.

A. Stabilizability for chaotic maps

Consider the two-dimensional neuromodule (3) discussed above and let x^* be some periodic orbit. The stability function describes local stability at x^*; cf. Figure 4. The region of stability in (α, μ)-parameter space is bounded by the lines $l_j(\alpha, \mu) = 1$ where $j = 1, 2$. The intersection of the half planes defined by the lines (8) gives the sector C_λ that describes stability around $(\alpha, \mu) = 0$ where $\lambda = (\lambda_1, \lambda_2)$ are the eigenvalues of $\mathrm{d}f_p|_{x^*}$; cf. Sec. III. Note that for fixed α,

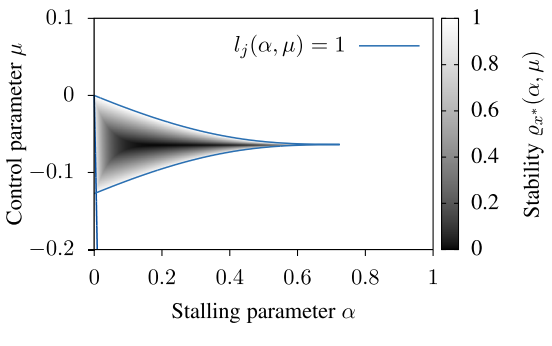

(a)

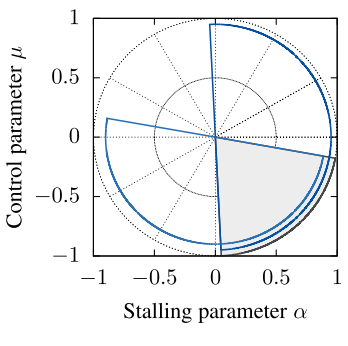

(b)

FIG. 4. Stability analysis for a periodic orbit of period $p = 5$ of the map (3) with local stability given by $\lambda = (\lambda_1, \lambda_2) = (1.46 \times 10^{-9}, 16.698)$ yields a region in parameter space in which it is stable. Panel (a) shows the stability function (7) and the lines defined by $l_j(\alpha, \mu) = 1$ with l_j as given by (6). The domain of stability C_λ around $(\alpha, \mu) = 0$ is depicted in panel (b). Note that this periodic orbit cannot be stabilized using the PFC method.

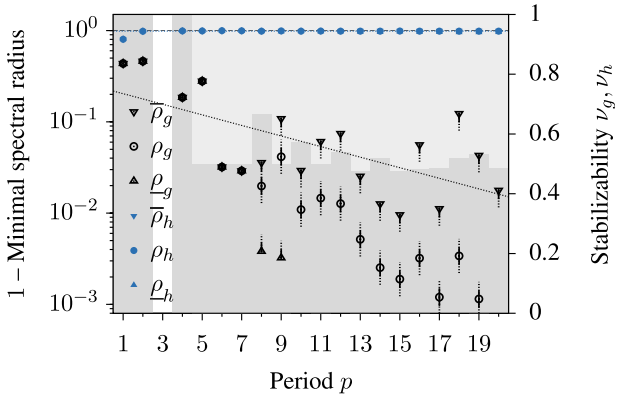

FIG. 5. Stalling PFC increases optimal asymptotic convergence speed for the 2D-neuromodule (3). SPFC yields period-independent asymptotic convergence speed. The shading indicates that more periodic orbits can be stabilized. The fraction of stabilizable orbits is shaded in gray; dark indicates stabilizability for both with and without stalling, light indicates stabilizability for SPFC only.

the range of μ which yields stability becomes smaller for larger α.

To compare the scaling of the spectral radius across periods, we plotted the functions (2) and (11) in Figure 5. The original PFC method exhibits asymptotic convergence speeds that approach one exponentially for increasing period. A fit of $\underline{\rho}$, corresponding to the best asymptotic convergence speed, by a function $\phi(x) = a\exp(-bx)$ yields a slope of $b = 0.1334$. By contrast, stalling the control significantly improves this scaling. We obtain values close to zero for all periods $p \in \{1, \ldots, 20\}$ and hence period-independent asymptotic convergence speed in terms of evaluations of f_p. A fit with an exponential function of $\underline{\rho}_h(p)$, i.e., the worst convergence speed, yields an exponent of $b = 3.8112 \times 10^{-8}$.

Qualitatively similar results are obtained for other two-dimensional chaotic maps,[17] such as the Hénon map[20] and the Ikeda map[21] (not shown).

As an example of a three-dimensional system, we analyzed a three-dimensional extension of the Hénon map[22] given by

$$f(x_1, x_2, x_3) = (a - x_2^2 - bx_3, x_1, x_2) \tag{13}$$

with parameters $a = 1.76$, $b = 0.1$. Stability properties of a periodic orbit of period $p = 6$ are depicted in Figure 6.

Due to additional constraints on stabilizability, the situation is different compared with the two-dimensional example above. In our example, the periodic orbits have a two-dimensional unstable manifold. If both eigenvalues corresponding to that manifold are real, the regime of stability depends on their sign and distance. If they have opposite signs, the periodic orbit cannot be stabilized, neither with nor without stalling. In case both eigenvalues have the same sign, the situation is depicted in Figure 6; there is a maximal value for α beyond which stabilization fails. For a pair of complex conjugate eigenvalues, the stability properties depend on the quotient of the real and imaginary part; cf. Figure 9. In particular, if the imaginary part is large, optimal asymptotic convergence speed is achieved for the PFC method, i.e., for a choice of $n = 0$.

When looking at the scaling of optimal asymptotic convergence speed across periods, we have to distinguish between even and odd periods (Figure 7). For even periods, we obtain a period-invariant scaling of both the mean and the best optimal asymptotic convergence speed similar to the two-dimensional system. While the upper bound on convergence speed will also increase to one due to the existence of periodic orbits with complex conjugate pairs, it will typically stay above the best convergence speed for the original PFC method. For odd periods, the number of periodic orbits with complex conjugate pairs of eigenvalues corresponding to the unstable directions is large. Therefore, we see the same performance as for the PFC method. Interestingly, for larger odd periods of $p > 10$ stalling becomes more effective at increasing optimal asymptotic convergence speed, boosting the best speed close to one.

A similar scaling behavior is present in other three-dimensional examples; period-independent scaling for even periods p is observed for a three-dimensional neuromodule[19] (not shown).

B. Convergence speed in applications

The scaling of the spectral radius indicates only the best possible asymptotic convergence speed for stalled predictive feedback control, i.e., the speed for the linearized dynamics. We ran simulations to compare the convergence speed for the full nonlinear system with the theoretical results for the linearized dynamics. In order to approximate a real-world implementation where control is turned on at a "arbitrary point in time," initial conditions were distributed randomly on the attractor according to the chaotic dynamics.

To evaluate convergence speed of stalled predictive feedback control, we compared the speed of $g_{\mu,p} = h^0_{\mu,p}$ with

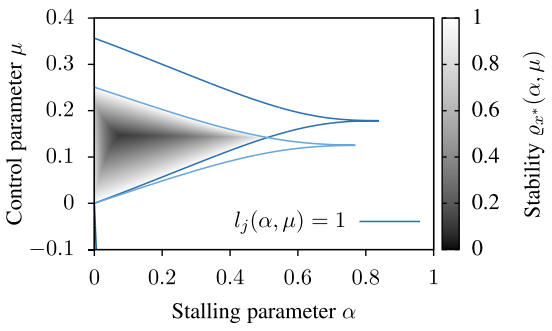

(a)

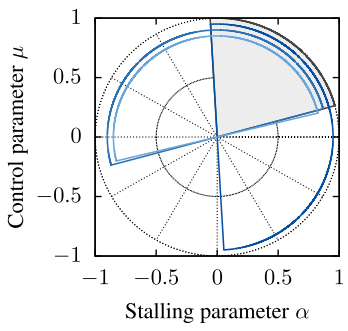

(b)

FIG. 6. Stability properties for a fixed point of period $p = 6$ of the three-dimensional Hénon map (13) with local stability given by $\lambda = (\lambda_1, \lambda_2, \lambda_3) = (3.1125 \times 10^{-8}, -4.6072, -6.9734)$ show a region where stabilization is successful. The stability function (7) is depicted in panel (a) and the domain of stability C_λ in panel (b), cf. Figure 4.

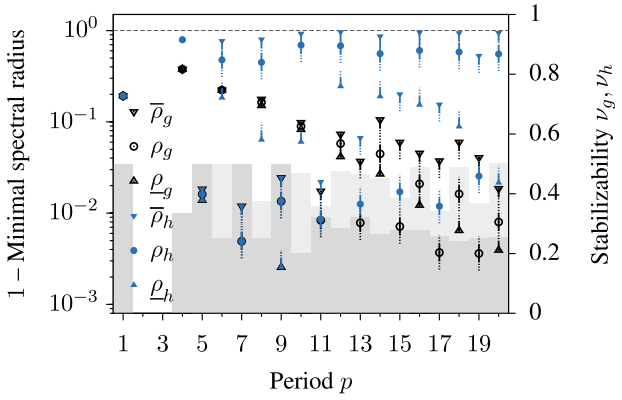

FIG. 7. Stalling predictive feedback control yields period-independent scaling for periodic orbits of even period for the three-dimensional Hénon generalization (13). Effectivity of stalling for odd periods increases with increasing period. The number of stabilizable periodic orbits (12) roughly doubles for higher periods as indicated by the shading, cf. Figure 5.

$h^{\alpha}_{\mu,p}$ for both $\alpha = 3^{-1}$ and $\alpha = (p+1)^{-1}$. In terms of the parameters m, n, a value of $\alpha = 3^{-1}$ corresponds to $m = 2$, $n = 1$, and $\alpha = (p+1)^{-1}$ to $m = p$, $n = 1$. In our implementation, convergence time is the time T for the dynamics to satisfy

$$\|x_T - \psi(x_T)\| \leq \theta_{\text{conv}}, \tag{14}$$

where ψ is one of the functions above. Convergence was only achieved if the criterion was fulfilled before a timeout of $T_{\text{timeout}} = 3000$ iterations. The convergence times were rescaled to evaluations of f_p to make them comparable. To calculate the best theoretical convergence time, we calculated the smallest spectral radius

$$\underline{\rho}^{\alpha}(p) = \min_{x^* \in \text{Fix}^*_h(f,p)} \inf_{\mu} \varrho(\mathrm{d}h^{\alpha}_{\mu,p}|_{x^*})$$

for all periodic orbits of a given period p with variable μ while keeping the stalling parameter $\alpha(m, n)$ fixed. By assuming $\|x^* - x_\tau\| = \|x^* - x_0\|(\underline{\rho}^{\alpha}(p))^{\tau}$ for the linear system, we have that for an initial separation of $\|x^* - x_0\| = d_{\text{ini}}$, the convergence criterion (14) is satisfied for

$$\tau^{\alpha}(p) = \left(\ln\left(\frac{\theta_{\text{conv}}}{d_{\text{ini}}}\right) - \ln\left(1 - \underline{\rho}^{\alpha}(p)\right)\right) \ln\left(\underline{\rho}^{\alpha}(p)\right)^{-1}. \tag{15}$$

Thus, $\tau^{\alpha}(p)$ is the convergence time of the linearized system for an initial condition x_0 with (period-independent) initial separation d_{ini}. For the simulations presented here, we chose $\theta_{\text{conv}} = 10^{-13}$ and $d_{\text{ini}} = 0.1$.

The results are shown in Figure 8. The errorbars depict mean and standard deviation for all 500 runs with initial conditions given by transient iteration of random length on the attractor. The value of the control parameter μ in the numerical simulations was chosen for each period to be the optimal value that yielded at least a fraction of 0.95 of convergent initial conditions. In other words, μ was chosen to yield the optimal speed with at least 95% reliability.

As predicted by the calculation of the spectral radius, stalling PFC leads to an increase in convergence speed across all periods. A scaling of convergence times (scaling is indicated by dashed lines) which is almost period-independent as observed in the theoretical calculations cannot be achieved in our simulations. This is due to several factors. First, in contrast to the linearized dynamics, the numerical simulations take the full nonlinear system into account. This includes the influence of the transient dynamics and the increasing complexity of the phase space (the number of fixed points increases with increasing period) on convergence times. Second, in the theoretical calculations, we consider only the fixed point for which convergence is fastest. However, even in our simulations, stalling improves both absolute convergence times was well as their scaling across periods compared with classical PFC. Furthermore, it increases the number of periods that can be stabilized. For some periods, only stalled predictive feedback control yields convergence within a reasonable time. The scaling of the convergence speeds is independent of whether the stalling parameter is fixed or scales with p. However, a period-dependent stalling parameter will generally reduce the standard deviation of the different convergence times.

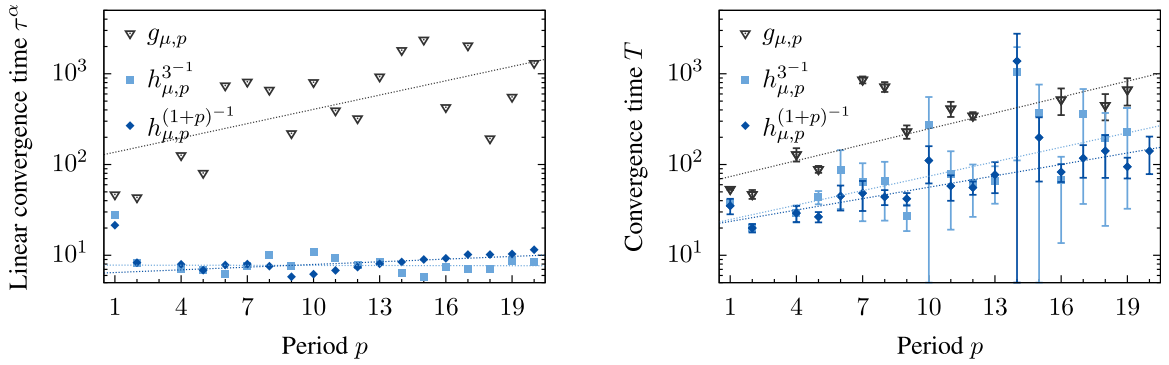

(a) (b)

FIG. 8. Although the best convergence times obtained from numerical simulations as shown in panel (b) cannot match the theoretical values of the linearized system given by (15), shown in panel (a), stalling PFC increases both the overall convergence times as well as the scaling across periods. Numerical simulations for the two-dimensional neuromodule (3) were performed with initial conditions distributed randomly on the chaotic attractor. Dashed lines represent an approximate exponential fit to indicating the overall scaling behavior.

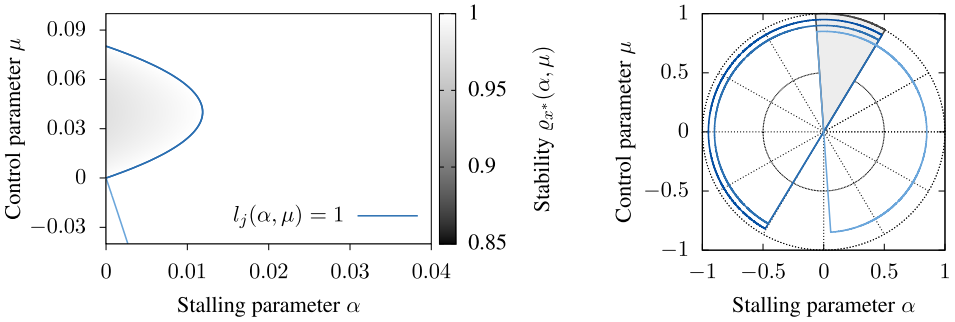

FIG. 9. For a period $p=5$ orbit of the three-dimensional Hénon map (13) with local stability properties $\lambda=(\lambda_1, \lambda_2, \lambda_3)=(0.0933+4.6673i, 0.0933-4.6673i, 0)$ with unstable directions given by a pair of complex conjugated eigenvalues, only few choices of the stalling parameter allow for stabilization (in particular, $m \gg 1$), cf. Figures 4 and 6. Optimal performance is achieved for the PFC method, i.e., with $n=0$.

C. Relation to earlier results

Stalled predictive feedback control as defined in Definition II.3 is a proper extension of the PFC method. In fact, the iteration of $h_{\mu,1}^{(1,1)}$ has been considered before in the context of predictive feedback control when trying to overcome the odd number limitation[23,24] as well as in the context of an experimental setup where measurements are time-delayed.[25] These studies were only concerned with whether or not fixed points can be stabilized, completely ignoring the aspect of convergence speed. Although for systems of dimension $N<3$, stalling control increases the number of fixed points that can be stabilized; even for $N=3$ there are points that can be stabilized using PFC but not using SPFC when the stalling parameter α is as large as in Refs. 23–25 (Figure 9). Hence, the introduction of an arbitrary stalling parameter is the key to both maximizing the number of fixed points subject to stabilization through PFC as well as minimizing the convergence speed.

The idea of periodically turning control on and off has been mentioned before in the literature on control theory; both "act-and-wait" control[26] and "intermittent" control[27] are stated for linear control problems in discrete and continuous time. At the same time, for linear control problems with many control parameters, "pole placement" techniques[28] are used to control the eigenvalues of the linearization. By contrast, SPFC aims at stabilizing many unstable periodic orbits of a given nonlinear system maintaining the simplicity of the simple one-parameter feedback control scheme. The situation where control is turned on at an arbitrary point in time as described above is of particular interest; here, the system is likely to be far from the linear regime. As shown above, stalling PFC improves performance even in this situation.

Stalling predictive feedback control is also related to a recent application of chaos control.[6] Because of implementation restraints, Steingrube *et al.* effectively iterated $f \circ g_{\mu,p}$. In some sense, this is similar to iterating $h_{\mu,p}^{(p,1)}$, but the stability analysis is not straightforward since one has to keep track of the (changing) point on the periodic orbit to be stabilized when iterating $f \circ g_{\mu,p}$. Moreover, both this control and SPFC are related to an effort by Polyak[8] to introduce a generalized PFC method, which is capable of stabilizing periodic orbits with an arbitrary small perturbation. This method, however, is limited in applicability, because the control perturbation depends on predictions of the state of the system many time steps in the future.

V. ADAPTIVE CONTROL

In Secs. III and IV, we showed that for an optimal choice of parameters, the asymptotic convergence speed of predictive feedback control can be significantly increased when stalling control. This speedup is not only of theoretical nature, but also persists in an implementation with random initial conditions. But how does one find the set of optimal parameter values for a given chaotic map f? If no *a priori* estimates are available, adaptation methods provide a way to tune the control parameters online for optimal convergence speed.

Here, we consider the case where the stalling parameter α (corresponding to some choice of m, n) is fixed and $\mu \geq 0$ is subject to adaptation. We explore different adaptation mechanisms and propose a hybrid gradient adaptation approach that leads to fast and highly reliable adaptation across different periods for initial conditions distributed randomly on the chaotic attractor.

A. Simple and gradient adaptation

First, recall a simple adaptation scheme.[6] We assume that the period p is fixed within this subsection. A suitable objective function for finding a periodic point of period p is given by

$$G_1(x,p) = \|f_p(x) - x\|^2$$

for some vector norm $\| \cdot \|$ on $\mathbb{R}^N$. For $\mu=0$, the map $h_{0,p}$ as defined in (5) reduces to some iterate of f and adaptation should lead to sequences $x_k \to x^*$ and $\mu_k \to \mu^*$ with $x^* \in \mathrm{Fix}(f_p)$ and $\varrho_h(\alpha, \mu^*) < 1$. The objective function above suggests a simple adaptation rule (SiA) rule with

$$\Delta\mu_k = \nu(p) G_1(x_k, p), \tag{16}$$

where $\nu(p)$ is the (possibly period-dependent) adaptation parameter and dynamics of μ given by

$$\mu_0 = 0, \quad \mu_{k+1} = \mu_k + \Delta\mu_k. \tag{17}$$

This adaptation rule increases the control parameter μ monotonically. Suppose that x^* is a fixed point of f, i.e.,

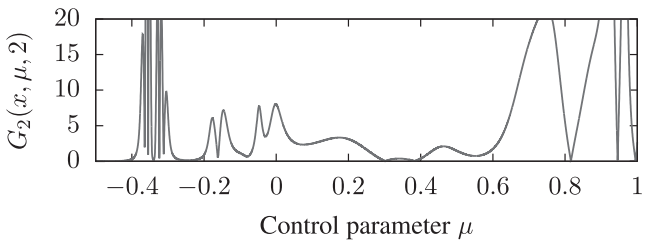

FIG. 10. The objective function $G_2(x, \mu, p)$ is nonconvex for a generic point x on the attractor leading to a difficult optimization problem.

$f_p(x^*) = x^*$. If we have a converging sequence $x_k \to x^*$ as $k \to \infty$ then the sequence $\Delta\mu_k$ tends to zero. In other words, adaptation stops in the vicinity of a fixed point x^* of f_p.

For this adaptation mechanism, the quantity $\Delta\mu_k$ is extremely easy to calculate and yields decent results in applications.[6] Adaptation, however, strongly depends on the choice of the adaptation parameter $\nu(p)$. If $\nu(p)$ is too small, it will take a long time to reach a regime in which convergence takes place. On the other hand, if $\nu(p)$ is too large and the interval M of possible values of μ in which convergence takes place is rather narrow, it is possible that $\mu_k > \sup M$ for some k, even if $\mu_l \in M$ for some values $l < k$. Hence, it is possible for the control parameter to "jump out of" the range of stability. Also, note that by construction, this simple adaptation will not optimize for asymptotic convergence speed. For small $\nu(p)$, adaptation will stop close to the boundary of the convergent regime, leading to slow asymptotic convergence speed; cf. Figure 11(a).

Adaptation may be improved, if the objective function takes local stability into account. For some matrix norm $\|\cdot\|$, such an objective function is given by

$$G_2(x, \mu, p) = \|\mathrm{d}h_{\mu,p}|_x\|.$$

Since any matrix norm is an upper bound for the spectral radius $\varrho(A)$ of a matrix A, that is, $\varrho(A) \le \|A\|$, minimizing the norm potentially leads to increased convergence speed.[16] At the same time, for a generic point on the attractor, this objective function is highly nonconvex with steep slopes (Figure 10) making straightforward minimization through, for example, gradient descent[29] difficult.

We therefore propose an adaptation rule that combines aspects of simple adaptation as reviewed above and the objective function G_2. Let ∂_μ denote the derivative with respect to μ and define $\Theta(x) = \tanh((pG_1(x,p))^{-1})$. Consider the modified gradient adaptation rule (GrA) rule given by (17) with

$$\Delta\mu_k = \lambda(p)(G_1(x,p) - p\,\tanh(\Theta(x_k)\partial_\mu G_2(h_{\mu,p}(x_k),\mu,p))). \tag{18}$$

This adaptation rule has the following properties. Far away from a period p orbit $x^* \in \mathrm{Fix}(f_p)$, i.e., for $G_1(x, p) \gg 0$, we have $\Theta(x) \approx 0$. Therefore, adaptation is dominated by the first term and leads to adaptation as given by the simple adaptation rule (16) to increase μ to reach a regime of convergence. On the other hand, in the vicinity of a fixed point, we have $\Theta(x) \approx 1$ and $G_1(x, p) \approx 0$. Hence, adaptation occurs by bounded gradient descent and the dynamics of the control parameter μ are perpendicular to the level sets of the objective function G_2 towards a (local) minimum. The bound induced by the tanh prevents large fluctuations of the objective function G_2 from leading to a too large change of the control parameter μ.

The adaptation parameter $\nu(p)$ again determines the size of the adaptation steps. In contrast to the simple adaptation method, the modified gradient adaptation adapts bidirectionally in order to minimize both objective functions G_1 and G_2 as depicted in Figure 11(a). Clearly, the control parameter is adapted to the regime of stability of a periodic orbit by the modified gradient adaptation and $\Delta\mu_k \to 0$ as optimal asymptotic convergence speed is achieved. Statistics for a large number of initial conditions show that the population mean $\langle\mu_k\rangle$ for many runs is already close to the optimal value after only 70 iterations; cf. Figure 11(b).

B. Convergence reliability

To assess the performance of the adaptive stalled predictive feedback chaos control algorithm in a real-world application, we performed large scale numerical simulations for the two-dimensional neuromodule (3). Periodic orbits were stabilized using SPFC (5) with the incorporation of the adaptation mechanisms given by (16) and (17). The scaling of the

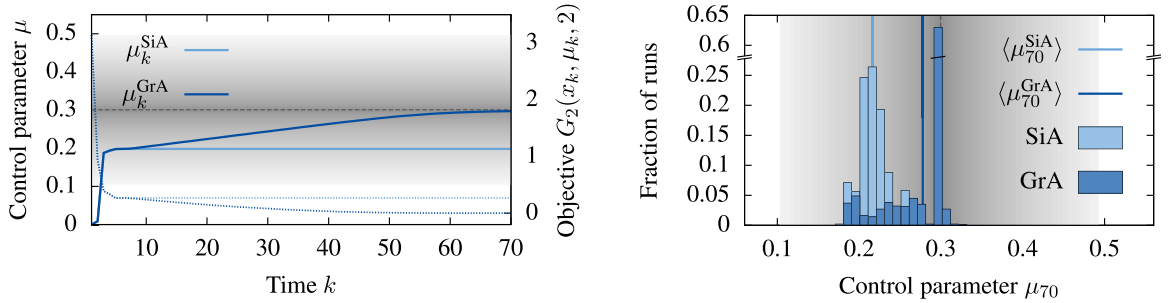

(a) (b)

FIG. 11. In contrast to simple adaptation, gradient adaptation tunes the control parameter to the value where optimal convergence speed is achieved. The dynamics for a single run are shown in panel (a) and the dotted lines depict the value of the objective function G_2. Statistics for 1000 initial conditions on the attractor after a transient of random length are shown in panel (b). The shading indicates values of the stability function smaller than one and the dashed line its minimum (optimal asymptotic convergence speed). The target period was $p = 2$ for the two-dimensional map (3) with adaptation parameter $\nu = 10^{-3}$ and $n = 1$, $m = 2$. Here, $\langle\cdot\rangle$ denotes the population mean.

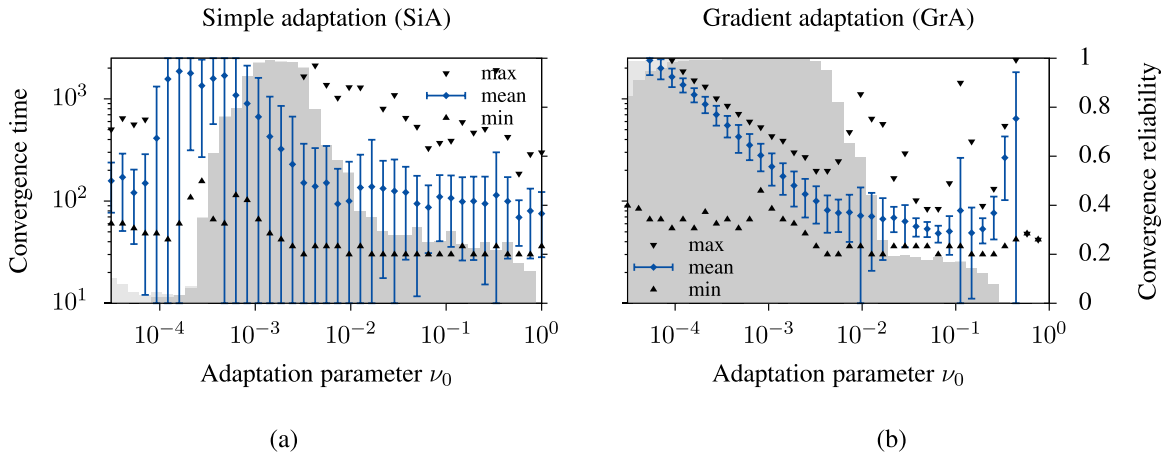

FIG. 12. Gradient adaptation (panel (b)) decreases the overall convergence times and the variation thereof compared with simple adaptation (panel (a)) for target period $p = 5$. Furthermore, the range of reliable convergence, depicted by the shading in the background, is broadened. The fraction of convergent runs to a periodic orbit of the correct period is shaded in dark gray (reliable convergence) and to an incorrect period in light gray.

adaptation parameter was given by $\nu(p) = \frac{\nu_0}{p}$ and for every ν_0, we iterated for 500 initial conditions distributed randomly on the chaotic attractor by iterating for a transient of random length. To determine reliability, i.e., the fraction of runs where the trajectory converged to a periodic orbit of the desired period, we checked the period of the limiting periodic orbit (if any) to a threshold of $\theta = 10^{-6}$.

As discussed above, the adaptation parameter ν_0 influences both speed and reliability. The results for period $p = 5$ are plotted in Figure 12. We find that gradient adaptation not only decreases the total number of time steps needed to fulfill the convergence criterion but it also decreases the overall variation across runs (the standard deviation is depicted as an error bar). Of particular interest for applications is the range where convergence is highly reliable. In contrast to the simple adaptation scheme, for gradient adaptation, the range of adaptation parameter values leading to highly reliable convergence is broadened. On the one hand, the gradient adaptation method optimizes for convergence speed, thereby increasing the chance that the convergence criterion is fulfilled before the timeout. At the same time, the bidirectional adaptation decreases the likelihood of the control parameter leaving the regime of convergence. Gradient adaptation therefore improves both overall convergence speed while reducing its variation and increasing the reliability of control.

The improvement of reliability compared with the simple adaptation scheme can be seen across all periods; cf. Figure 13. The broad range of adaptation parameters giving highly reliable convergence allows for the choice of an adaptation parameter ν_0 that will lead to reliable convergence across different periods, effectively eliminating this parameter.

Similar results are obtained for numerical simulations for other two- as well as three-dimensional chaotic maps (not shown). These include the Hénon map[17] and a three-dimensional neuromodule.[19] Convergence speed of μ_k to the optimal parameter value can be further increased by using higher order methods, such as Newton's method (not shown). The use of higher order methods (also with respect to comparing simple and gradient adaptation) comes with a higher absolute computational cost. For any implementation, the improvement always needs to be related to the effective improvement.

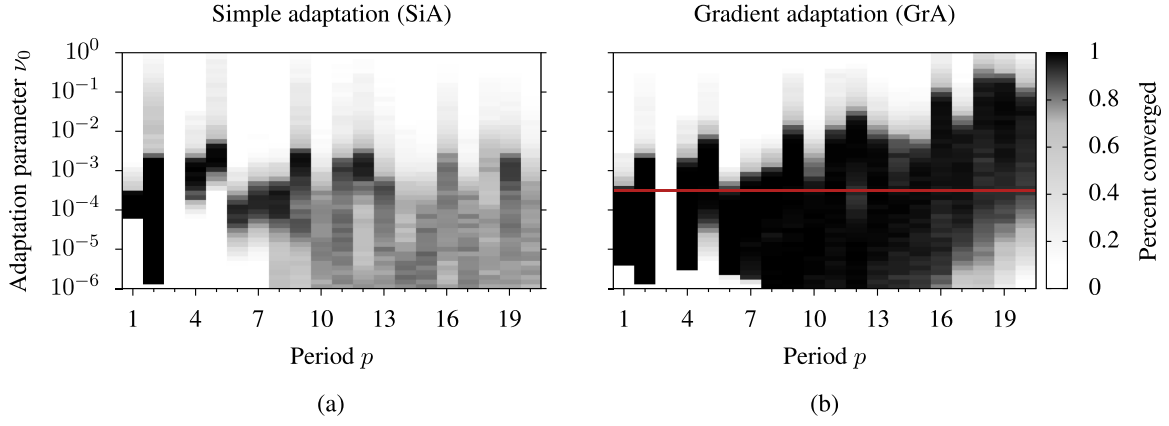

FIG. 13. Gradient adaptation (panel (b)) increases the overall reliability of convergence across periods compared with simple adaptation (panel (a)). Reliability, i.e., the percentage of convergent runs to periodic orbits of the target period p, is depicted by the color of the shading for the adaptation parameter ν_0 and hence more dark areas correspond to higher overall reliability. For gradient adaptation, there exist parameter values which yield reliable convergence across all periods ($\nu_0 = 10^{-3.5}$ is depicted by a red line).

VI. DISCUSSION

In this article, we studied the effect stalling has on predictive feedback control. By stalling control, the inherent speed limit of standard predictive feedback control may be overcome. We highlighted that only by taking all possible stalling parameters into account, the maximum number of periodic orbits can be stabilized. The conditions on stabilizability that we derived show that stabilizability is reduced to the conditions imposed by the eigenvalues corresponding to the unstable directions. Stalling is very easy to implement and, in addition to increasing convergence speed, the resulting chaos control method is capable of stabilizing more periodic orbits. Combined with targeting algorithms,[30] SPFC can also be used to stabilize specific periodic orbits. Using numerical simulations, we showed that in applications where chaos control is turned on at a random point in time, convergence speed is greatly improved across all periods. Although our method was stated in terms of discrete time dynamical systems, it also applies to continuous time dynamics if discretized, for example, through a Poincaré map.

As examples, we studied "typical" low-dimensional chaotic systems. In higher dimensions, for example, when studying chaotic collective effects in networks, we expect our method to behave qualitatively similar as in the three-dimensional case, although an increase in dimension of the unstable manifold of periodic orbits places additional constraints on stabilizability. *A priori* estimates of the local stability properties of the periodic orbits embedded in the attractor yield an estimate of how many periodic orbits can be stabilized. This limitation could be overcome by tuning the eigenvalue corresponding to some eigenvector separately. From a mathematical point of view, a different approach would be to allow the control parameter to take complex values, turning the problem into one of complex dynamics in several complex variables.[16] On the other hand, the local stability property conditions provide design principles for attractors to contain many unstable periodic orbits that our stalled predictive feedback control method is capable of stabilizing. These important questions, however, are beyond the scope of the current article and will have to be addressed in further research.

Conversely, the local stability properties and the narrowing of the regime of stability for the control parameter μ while $\alpha > 0$ is fixed can actually be exploited. Different local stability properties of the unstable periodic orbits allow for stabilization of a specific set of periodic orbits. Hence, through the choice of parameters, the targeted periodic orbits can become stable periodic orbits of the dynamics.

Adaptation mechanisms not only provide a way to tune the adaptation parameter to a suitable value, but they also allow for an increase in both speed and reliability. In contrast to previously proposed adaptation,[6,31] the proposed hybrid algorithm also adapts for optimal convergence speed. A broad range of parameters allows for a period-independent choice of adaptation parameter, hence giving a chaos control method with a set of parameters for which it stabilizes many periodic points of most periods quickly and reliably. Adaptation using the objective function (16) also prevents the system from converging to one of the periodic orbits potentially induced by stalling control. However, as our adaptation method merely serves as a proof of concept, it still leaves room for improvement. In particular, the cap of adaptation speed through the sigmoidal function is a major source of slowdown. Moreover, adaptation could be extended to the stalling parameter α.

Since stalling PFC increases the number of evaluations of f_p needed for a single iteration of $h_{p,\mu}$, it would be desirable to extend the theory to a "fractional stalling parameter," i.e., to allow for stalling by composing with $f^{\circ q}$ where $q < p$. With such stalling, however, one needs to track the point of the periodic orbit, as discussed in Sec. IV C, rendering the theoretical analysis more subtle.

In conclusion, stalled predictive feedback control of chaos together with a suitable adaptation scheme is a step towards a fast, reliable, easy-to-implement, and broadly applicable chaos control method. It would be interesting to see it applied in experimental setups in the future.

ACKNOWLEDGMENTS

The authors would like to thank E. Schöll and A. Fradkov for helpful discussions. C.B. would like to thank Laurent Bartholdi for making this project possible. This work was supported by the Federal Ministry of Education and Research (BMBF) by Grant Nos. 01GQ1005A and 01GQ1005B.

[1]A. Katok and B. Hasselblatt, *Introduction to the Modern Theory of Dynamical Systems* (Cambridge University Press, Cambridge, UK, 1995), p. xviii, 802.
[2]E. Ott, C. Grebogi, and J. A. Yorke, "Controlling chaos," Phys. Rev. Lett. **64**, 1196 (1990).
[3]M. I. Rabinovich and H. D. I. Abarbanel, "The role of chaos in neural systems," Neuroscience **87**, 5 (1998).
[4]*Handbook of Chaos Control*, edited by E. Schöll and H. G. Schuster (Wiley-VCH Verlag, Weinheim, Germany, 1999).
[5]A. Garfinkel, M. Spano, W. Ditto, and J. Weiss, "Controlling cardiac chaos," Science **257**, 1230 (1992).
[6]S. Steingrube, M. Timme, F. Wörgötter, and P. Manoonpong, "Self-organized adaptation of a simple neural circuit enables complex robot behaviour," Nat. Phys. **6**, 224 (2010).
[7]M. de Sousa Vieira and A. Lichtenberg, "Controlling chaos using nonlinear feedback with delay," Phys. Rev. E **54**, 1200 (1996).
[8]B. T. Polyak, "Stabilizing chaos with predictive control," Autom. Remote Control **66**, 1791 (2005).
[9]K. Pyragas, "Continuous control of chaos by self-controlling feedback," Phys. Lett. A **170**, 421 (1992).
[10]P. Schmelcher and F. K. Diakonos, "Detecting unstable periodic orbits of chaotic dynamical systems," Phys. Rev. Lett. **78**, 4733 (1997).
[11]P. Schmelcher and F. K. Diakonos, "General approach to the localization of unstable periodic orbits in chaotic dynamical systems," Phys. Rev. E **57**, 2739 (1998).
[12]D. Pingel, P. Schmelcher, F. K. Diakonos, and O. Biham, "Theory and applications of the systematic detection of unstable periodic orbits in dynamical systems," Phys. Rev. E **62**, 2119 (2000).
[13]J. J. Crofts and R. L. Davidchack, "Efficient detection of periodic orbits in chaotic systems by stabilizing transformations," SIAM J. Sci. Comput. **28**, 1275 (2006).
[14]B. Doyon and L. Dubé, "Targeting unknown and unstable periodic orbits," Phys. Rev. E **65**, 037202 (2002).
[15]R. L. Davidchack and Y.-C. Lai, "Efficient algorithm for detecting unstable periodic orbits in chaotic systems," Phys. Rev. E **60**, 6172 (1999).
[16]C. Bick, M. Timme, and C. Kolodziejski, "Adapting predictive feedback chaos control for optimal convergence speed," SIAM J. Appl. Dyn. Syst. **11**, 1310 (2012).

[17]C. Bick, C. Kolodziejski, and M. Timme, "Stalling chaos control accelerates convergence," New J. Phys. **15**, 063038 (2013).
[18]P. Cvitanović, R. Artuso, R. Mainieri, G. Tanner, and G. Vattay, *Chaos: Classical and Quantum* (Niels Bohr Institute, Copenhagen, 2012).
[19]F. Pasemann, "Complex dynamics and the structure of small neural networks," Network **13**, 195 (2002).
[20]M. Hénon, "A two-dimensional mapping with a strange attractor," Commun. Math. Phys. **50**, 69 (1976).
[21]K. Ikeda, H. Daido, and O. Akimoto, "Optical turbulence: Chaotic behavior of transmitted light from a ring cavity," Phys. Rev. Lett. **45**, 709 (1980).
[22]G. Baier and M. Klein, "Maximum hyperchaos in generalized Hénon maps," Phys. Lett. A **151**, 281 (1990).
[23]H. G. Schuster and M. Stemmler, "Control of chaos by oscillating feedback," Phys. Rev. E **56**, 6410 (1997).
[24]O. Morgül, "Stabilization of unstable periodic orbits for discrete time chaotic systems by using periodic feedback," Int. J. Bifurcation Chaos Appl. Sci. Eng. **16**, 311 (2006).
[25]J. C. Claussen and H. G. Schuster, "Improved control of delayed measured systems," Phys. Rev. E **70**, 056225 (2004).
[26]T. Insperger and G. Stépán, "Act-and-wait control concept for discrete-time systems with feedback delay," IET Control Theory Appl. **1**, 553 (2007).
[27]P. Gawthrop, "Act-and-wait and intermittent control: Some comments," IEEE Trans. Control Syst. Technol. **18**, 1195 (2010).
[28]E. D. Sontag, *Mathematical Control Theory* (Springer-Verlag, New York, 1998), p. xvi + 531.
[29]A. L. Fradkov and A. Y. Pogromsky, *Introduction to Control of Oscillations and Chaos* (World Scientific, 1998), p. 391.
[30]E. J. Kostelich, "Targeting in chaotic dynamical systems," in *Handbook of Chaos Control*, edited by Heinz G. Schuster (Wiley-VCH Verlag, 1999), pp. 141–156.
[31]J. Lehnert, P. Hövel, V. Flunkert, P. Y. Guzenko, A. L. Fradkov, and E. Schöll, "Adaptive tuning of feedback gain in time-delayed feedback control," Chaos **21**, 043111 (2011).